Amplified Heavy-Atom Free Phosphorescence from *Meta*-Dimethoxy Difluoroboron β–Diketonate Charge-Transfer Materials

Christopher A. DeRosa, Satoru Hiroto,† Cassandra L. Fraser*

Department or Chemistry, University of Virginia, McCormick Road, Charlottesville VA, 22904, USA

ABSTRACT

Difluoroboron β–diketonate materials are used for biomedical oxygen sensing applications. These fluorophores show both fluorescence (F) and phosphorescence (P) when the dye is embedded in a polymer matrix. The fluorescence is insensitive to oxygen quenching, while the phosphorescence changes intensity dependent on the oxygen concentration. This enables oxygen quantification by ratiometric methods with good spatial and temporal resolution. Here, we produce ratiometric-capable oxygen sensors without the need of a heavy atom. This is achieved by substituting methoxyl groups at the *meta*-positions of an aromatic ring, dramatically influencing the electronic transitions of the fluorophore. Altering the aromatic group on the opposing ring tailors the absorption wavelength, luminescence colors and relative fluorescence to phosphorescence ratio

(F/P), important for oxygen sensing. The phosphorescence lifetimes are also hundreds of milliseconds long, achieving ultra-sensitivity to oxygen. This study presents the synthesis, optical characterization in solution and polylactide blends, and computational analysis of 3,5-dimethoxy-difluoroboron β–diketonate materials as oxygen sensing materials.

INTRODUCTION

Luminescent materials are employed as imaging agents and optical devices for lighting and energy.[1–6] Fluorescence (F), room-temperature phosphorescence (RTP), and thermally-activated delayed fluorescence (TADF) all play important roles in the design of functional materials.[7] In cellular imaging, bright fluorophores with high quantum yields, long luminescence lifetimes and good photostabilities are ideal for organelle tagging, sensing and long-term tracking.[8,9] Therefore, fluorophores with these desired properties are under intense investigation.[10] Simple changes in molecular structure can yield next generation optical materials. Boron modified materials and boron β–diketonate dyes are bright, multi-photon excitable, medium-sensitive fluorophores useful for a growing number of applications.[11–20] Beyond the fluorescence properties of these dyes, emission from the triplet state can also be achieved in the form of TADF and RTP when the dyes are embedded into a rigid matrix (e.g. polylactic acid).[21,22] This was initially discovered for the dye-polymer conjugate difluoroboron dibenzoylmethane-PLA (BF$_2$dbmPLA).[23] PLA is a biodegradable polymer that is readily processed for different biomedical applications.[24–27]

The multi-emissive properties of these materials are beneficial for many uses such as OLEDs,[28–31] long-lifetime imaging probes,[32–36] and oxygen sensors.[37–44] Because the fluorescence and phosphorescence originate from a single dye, or polymeric material, complications due to dye mixing are circumvented (i.e. fluorescent dye + phosphorescent dye).[45–47] The fluorescence, un-

quenched by oxygen, serves as an internal standard, while the oxygen-sensitive phosphorescence is can report the relative oxygen concentration. Thus, ratiometric oxygen sensing is achievable with a single dye. In most purely organic materials, the fluorescence is significantly stronger than the phosphorescence,[23,48–51] but dyes have been prepared to shift the balance towards stronger phosphorescence. One strategy exploits the heavy-atom effect, which increases the rate of intersystem crossing via spin-orbit coupling.[52] In organic molecules, this can be observed by measuring the phosphorescence in heavy-atom enriched solvents, such as iodomethane, for an external heavy atom effect.[53,54] A more practical method is introduction of a halide, such as iodide or bromide, to the molecular structure to cause an internal heavy-atom effect.[55–57] This has been demonstrated for difluoroboron β–diketonate ratiometric oxygen sensors,[58,59] benzo[2,1,3]thiadiazoles,[60] N-substituted naphthalimides,[61–63] and bromine-substituted benzaldehyde-based phosphors.[64,65] The greatest drawback to heavy-atom induced phosphorescence is reduced photostability.[66] Also, for oxygen-sensing applications, the oxygen sensitivity is greatly reduced.[49] While this can be beneficial for certain applications,[44] maintaining phosphorescence with long lifetimes and ultrasensitivity to oxygen can be challenging via heavy atom placement.

Recently, there has been progress in the preparation of heavy-atom free oxygen sensors. Zhang et al., reported a set of *N*-substituted naphthalimides (NNI) with strong orange-red phosphorescence achieved via the introduction of electron rich aromatics to increase charge transfer.[62] Challenges for NNI-based oxygen sensors arise from the low quantum yields. Also notable are some heavy-atom free difluoroboron β–diketonate complexes reported by Klimant and coworkers. These ultrasensitive difluoroboron 9-hydroxyphenalenone chelates (BF$_2$HPhN) were employed as oxygen sensors with exceptional properties, such as distinct fluorescence and

phosphorescence wavelengths, long phosphorescence lifetimes and thermally activated fluorescence.[67,68] However, the large π–aromatic systems of BF_2HPhN dyes resulted in poor matrix solubility and reduced photostability.[68] Therefore, new techniques for enhancing the phosphorescence without resorting to heavy-atom substitution or large aromatic moieties have not yet been realized.

In this report, we build upon knowledge of charge transfer in BF_2bdks to design new oxygen sensitive materials with intense phosphorescence. Previously we reported that the difluoroboron moiety plays a key role in activating the phosphorescence emission by restricting molecular motions and enhancing the donor-acceptor property of the diketonate.[69,70] We hypothesize that the phosphorescence intensity may be linked to the charge separation, namely, the charge transfer (CT) of the molecule.[71] This has been demonstrated in a recent report of naphthyl-phenyl systems, with and without bromide substituents, to increase the phosphorescence intensity.[72,73] This is also supported in a study of dibenzoylmethane derivatives, where *meta*-alkoxy substitution led to increased charge transfer properties and intensified phosphorescence.[74] However, a heavy atom was still required to enable strong phosphorescence, a prerequisite for ratiometric oxygen sensing. Also, altering the polymer matrix (e.g. polystyrene or poly(methyl methacrylate)) had little influence on the phosphorescence intensity. Therefore, we propose that further increasing the CT character with two alkoxy groups at the *meta*-position of the aromatic ring can eliminate the necessity of the heavy atom, producing more photostable, ultrasensitive oxygen sensors. Galer and coworkers were the first to present a 3,5-dimethoxybenzene-dibenzolymethane boron difluoride (difluoroboron-1-phenyl-3-(3,5-dimethoxyphenyl)-propane-1,3-dione), which displayed a variety of fluorochromic behaviors, such as mechanochromism, solvatochromism, thermochromism and chronochromism (Figure 1, compound **1**).[75] Density

functional theory (DFT) properties of this dye showed strong charge-transfer properties. Thus, we hypothesize that this dye scaffold is an the ideal candidate for enhanced RTP via charge-transfer.[62] Galer and coworkers investigated the solid state properties of **1** extensively, but the phosphorescence of these types of compounds in polymers is unknown. Here, we test the RTP properties of a series of 3,5-dimethoxybenzoyl dyes with variable aromatic groups (Figure 1). The charge separation is generated by an electron localized highest occupied molecular orbital (HOMO) and an electron-delocalized lowest unoccupied molecular orbital. Varying aromatic groups (e.g. phenyl, naphthyl and thienyl) can be used to modulate the degree of charge transfer, luminescence colors, and phosphorescence lifetimes.
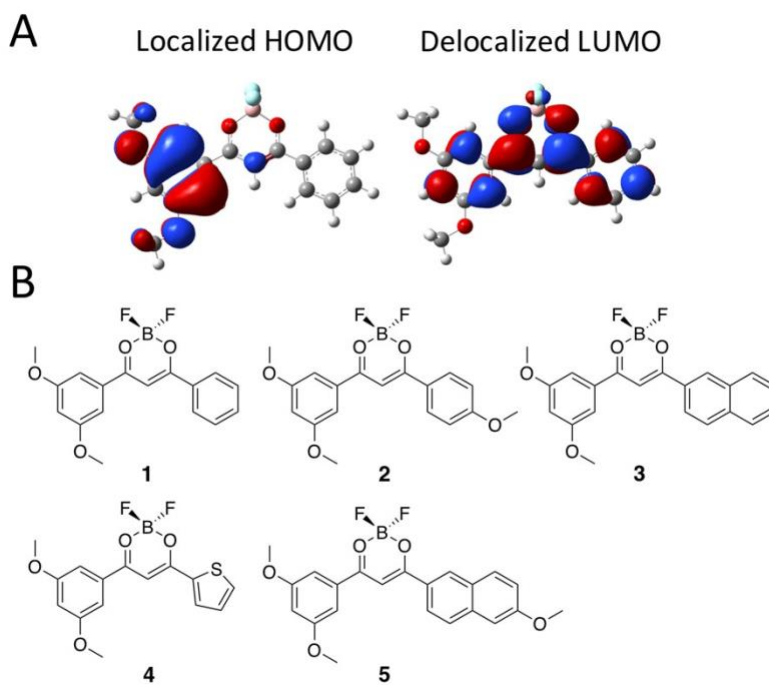

Figure 1. Molecular Design of Charge Transfer Difluoroboron β–Diketonates. A) Distribution of electron density within the 3,5-dimethoxy substituted dibenzoylmethane dye (**1**) showing strong CT character. (See calculation data in the Supporting Information).[75] B) Chemical structures of dyes in this work.

This study describes dye synthesis, optical properties in solution, theoretical study, and the oxygen sensing properties of the dyes embedded in PLA. All the dyes show strong

phosphorescence in PLA blends, enabling heavy atom free, ratiometric oxygen sensing. Furthermore, with ultralong phosphorescence, these materials maintain highly sensitive oxygen-sensing properties,[67,76–78] ideal for industrial applications (i.e. trace oxygen analyzers) and extreme hypoxic or anoxic environments (e.g. in tumors).[41,79]

EXPERIMENTAL SECTION

Materials. Solvents CH_2Cl_2 and THF were dried over 3 Å molecular sieves activated at 300 °C, transferred via cannula, and dried a second time over 3 Å molecular sieves activated at 300 °C.[80] The solvents were stored in a dry pot. All other chemicals were reagent grade from Sigma-Aldrich and were used without further purification. The ligand,1-(3,5-dimethoxyphenyl)-3-hydroxy-3-phenylprop-2-en-1-one (**L1**), and boron dye, difluoroboron-1-(3,5-dimethoxyphenyl)-3-oxo-3-phenylprop-2-en-1-one (BF_2 3, 5-OMe-dbm; **1**) were prepared as previously described by Galer et al.[75] ^{1}H NMR spectra are in accordance with literature values.

Methods. ^{1}H NMR spectra (600 MHz) were recorded on a Varian VMRS 600/51 instrument in $CDCl_3$ or d_6-DMSO. ^{1}H NMR spectra were referenced to the residual signals for protiochloroform (7.26 ppm). In the ^{1}H NMR assignments, aromatic positions are defined for phenyl (Ar), naphthyl, (Np), and thienyl (Th). Coupling constants are given in hertz. UV−vis spectra were recorded on a Hewlett-Packard 8452A diode-array spectrophotometer. The β–diketonate ligands were prepared as previously described using methyl 3,5-dimethoxybenzoate with the corresponding aromatic ketone, 1-(4-methoxyphenyl)ethan-1-one (**L2**), 1-(naphthalen-2-yl)ethan-1-one (**L3**), 1-(thiophen-2-yl)ethan-1-one (**L4**), and 1-(6-methoxynaphthalen-2-yl)ethan-1-one (**L5**) in the presence of NaH (60% in oil) as a base.[81] Boron dyes were prepared as previously described with the corresponding ligands. Ligands and dyes were purified by recrystallization from

acetone/hexanes until ^{1}H NMR revealed high purity. The compound yields, ^{1}H NMR (Figures S8-S16) and mass spectroscopy data are provided.

Luminescence Measurements. Steady-state fluorescence emission spectra were recorded on a Horiba Fluorolog-3 Model FL3-22 spectrofluorometer (double-grating excitation and double-grating emission monochromator). A 2 ms delay was used when recording the delayed emission spectra. Time-correlated single-photon counting (TCSPC) fluorescence lifetime measurements were performed with a NanoLED-370 (λ_{ex} = 369 nm) excitation source and a DataStation Hub as the SPC controller. Phosphorescence lifetimes were measured with a 1 ms multichannel scalar (MCS) excited with a flash xenon lamp (λ_{ex} = 369 nm; duration <1 ms). Lifetime data were analyzed with DataStation v2.4 software from Horiba Jobin Yvon. Fluorescence quantum yields (Φ_F) of initiator and polymer samples in CH_2Cl_2 were calculated against anthracene as a standard as previously described, using the following values: Φ_F (Quinine sulfate) = 0.546,[82] (0.1 M H_2SO_4) = 1.380, n_D^{20} (CH_2Cl_2) = 1.424. Optically dilute CH_2Cl_2 solutions of the dyes, with absorbances <0.1 au, were prepared in 1 cm path length quartz cuvettes. Fluorescence spectra and lifetimes were obtained under ambient conditions (e.g., air, ~21% oxygen). Phosphorescence measurements were performed under a N_2 atmosphere. Vials were continuously purged in the headspace between the solution and the vial cap with analytical grade N_2 (Praxair) during measurements with a 12 mm PTFE/silicone/PTFE seal (Chromatography Research Supplies), connected by a screw cap. For 21% O_2 (i.e. air), measurements were taken under ambient conditions (open vial, no cap). Oxygen calibration was performed as previously described with Cole-Palmer flow gauges with mixtures of O_2 and N_2 (Praxair) gases.[59] Fluorescence and phosphorescence lifetimes were fit to double exponential decays in PLA films. Fluorescence lifetimes in CH_2Cl_2 were fit to single exponential decays. Solvatochromism measurements were

performed as previously described with spectroscopic grade organic solvents (hexane, toluene, methylene chloride, acetone and acetonitrile) at constant concentration (~10^{-5} M).[14]

β–Diketones

1-(3,5-Dimethoxyphenyl)-3-hydroxy-3-(4-methoxyphenyl)prop-2-en-1-one (3,5-OMe-dbm-OMe; **L2**). The ligand was isolated as an off-white crystalline solid (760 mg, 71%). ^{1}H NMR: (600 MHz, DMSO) δ 17.33 (s, 1H, enol-*H*), 8.16 (d, J = 12, 2H, 2, 6-OMeAr*H*), 7.23 (s, 2H, 2, 6-MetaAr*H*), 7.21 (s, 1H, COC*H*CO), 7.07 (d, J = 12, 2H, 3, 5-OMeAr*H*), 6.73 (s, 1H, 4-MetaAr*H*), 3.84 (s, 3H, 4-OMeArOC*H₃*), 3.82 (s, 6H, 3,5-MetaArOC*H₃*). HRMS (ESI, TOF) m/z calcd for $C_{18}H_{18}BO_5F_2$: 363.1215 $[M + H]^+$; found 363.1225. HRMS (ESI, TOF) m/z calcd for $C_{18}H_{19}O_5$: 315.1232 $[M + H]^+$; found 315.1234.

1-(3,5-Dimethoxyphenyl)-3-hydroxy-3-(naphthalen-2-yl)prop-2-en-1-one (3,5-dimethoxy-bnm; **L3**). The ligand was isolated a tan crystalline solid (1.4 g, 54%). ^{1}H NMR: (600 MHz, DMSO) δ 17.23 (s, 1H, enol-*H*), 8.84 (s, 1H, 1-Np*H*), 8.25-8.00 (m, 4H, 3, 4, 5, 8-Np*H*), 7.68-7.60 (m, 2H, 6, 7-Np*H*), 7.45 (s, 1H, COC*H*CO), 7.27 (s, 2H, 2, 6-MetaAr*H*), 6.71 (s, 1H, 4-MetaAr*H*), 3.84 (s, 6H, 3,5-MetaArOC*H₃*). HRMS (ESI, TOF) m/z calcd for $C_{21}H_{19}O_4$: 335.1283 $[M + H]^+$; found 335.1299.

1-(3,5-Dimethoxyphenyl)-3-hydroxy-3-(thiophen-2-yl)prop-2-en-1-one (3,5-OMe-btm; **L4**). The ligand was isolated a brown crystalline solid (243 mg, 15%). ^{1}H NMR: (600 MHz, DMSO) δ 16.44 (s, 1H, enol-*H*), 8.34 (d, J = 6, 1H, 5-Th*H*), 8.04 (d, J = 6, 1H, 3-Th*H*), 7.29 (t, J = 6, 1H, 4-Th*H*), 7.19 (s, 2H, 2, 6-MetaAr*H*) 7.03 (s, 1H, COC*H*CO), 6.73 (s, 1H, 4-MetaAr*H*), 3.81 (s, 6H, 3,5-MetaArOC*H₃*). HRMS (ESI, TOF) m/z calcd for $C_{15}H_{15}O_4S$: 291.0691 $[M + H]^+$; found 291.0692.

1-(3,5-Dimethoxyphenyl)-3-hydroxy-3-(6-methoxynaphthalen-2-yl)prop-2-en-1-one (3,5-dimethoxy-bnmOMe; **L5**). The ligand was isolated an off-white powder (450 mg, 30%). ^{1}H NMR: (600 MHz, DMSO) δ 17.31 (s, 1H, enol-*H*), 8.77 (s, 1H, 1-OMeNp*H*), 8.16 (d, J = 6, 1H, 3-OMeNp*H*), 8.03 (d, J = 12, 1H, 8-OMeNp*H*), 7.94 (d, J = 12, 1H, 7-OMeNp*H*), 7.43 (s, 1H, 5-OMeNp*H*), 7.41 (s, 1H, COC*H*CO), 7.28 (s, 2H, 2, 6-MetaAr*H*), 7.25 (d, J = 6, 1H, 4-OMeNp*H*), 6.79 (s, 1H, 4-MetaAr*H*), 3.90 (s, 3H, 6-OMeNpOC*H₃*), 3.84 (s, 6H, 3,5-MetaArOC*H₃*). HRMS (ESI, TOF) m/z calcd for $C_{22}H_{21}O_5$: 365.1389 [M + H]$^+$; found 365.1407.

Boron Dyes

BF$_2$-3,5-dimethoxy-dbmOMe (**2**). The dye was isolated as a yellow powder (135 mg, 86%). ^{1}H NMR: (600 MHz, DMSO) δ 8.40 (d, J = 6, 2H, 2, 6-OMeAr*H*), 7.78 (s, 1H, COC*H*CO), 7.41 (s, 2H, 2, 6-MetaAr*H*) 7.18 (d, J = 6, 2H, 3, 5-OMeAr*H*), 6.90 (s, 1H, 4-MetaAr*H*), 3.92 (s, 3H, 4-OMeArOC*H₃*), 3.85 (s, 6H, 3,5-MetaArOC*H₃*). HRMS (ESI, TOF) m/z calcd for $C_{18}H_{18}BO_5F_2$: 363.1215 [M + H]$^+$; found 363.1225.

BF$_2$-3,5-dimethoxy-bnm (**3**). The dye was isolated as a yellow powder (361 mg, 68%). ^{1}H NMR: (600 MHz, DMSO) δ 9.13 (s, 1H, 1-Np*H*), 8.36 (d, J = 6, 1H, 8-Np*H*), 8.21 (d, J = 12, 1H, 3-Np*H*), 8.14 (d, J =12, 1H, 4-Np*H*), 8.06 (s, 1H, COC*H*CO), 7.76 (t, J = 6, 1H, 6-Np*H*), 7.68 (t, J = 6, 1H, 7-Np*H*), 7.49 (s, 2H, 2, 6-MetaAr*H*), 6.95 (s, 1H, 4-MetaAr*H*), 3.88 (s, 6H, 3,5-MetaArOC*H₃*). HRMS (ESI, TOF) m/z calcd for $C_{21}H_{18}BO_4F_2$: 383.1266 [M + H]$^+$; found 383.1258.

BF$_2$-3,5-dimethoxy-btm (**4**). The dye was isolated as a dark yellow powder (56 mg, 76%). ^{1}H NMR: (600 MHz, DMSO) δ 8.74 (s, broad, 1H, 5-Th*H*), 8.41 (s, broad, 1H, 3-Th*H*), 7.80 (s, 1H, COC*H*CO), 7.48 (t, J = 6, 1H, 4-Th*H*), 7.38 (s, 2H, 2, 6-MetaAr*H*), 6.92 (s, 1H, 4-MetaAr*H*), 3.85
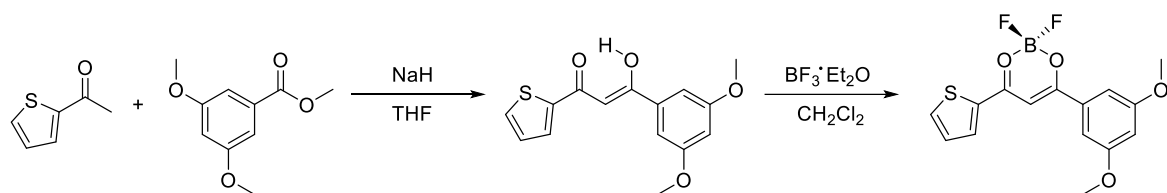
(s, 6H, 3,5-MetaArOCH_3). HRMS (ESI, TOF) m/z calcd for C$_{15}$H$_{14}$BO$_4$F$_2$S: 339.0674 [M + H]$^+$; found 339.0680.

BF$_2$-3,5-dimethoxy-bnmOMe (**5**). The dye was isolated as an orange powder (134 mg, 43%). ^{1}H NMR: (600 MHz, DMSO) δ 9.06 (s, 1H, 1-OMeNpH), 8.33 (d, J = 6, 1H, 8-OMeNpH), 8.12 (d, J = 6, 1H, 3-OMeNpH), 8.01 (d, 1H, J = 6, 1H, 4-OMeNpH), 7.96 (s, 1H, COCHCO), 7.50 (s, 1H, 5-OMeNpH), 7.46 (s, 2H, 2, 6-MetaArH), 8.32 (d, J = 6, 1H, 7-OMeNpH), 6.94 (s, 1H, 4-MetaArH), 3.94 (s, 3H, 6-OMeNpOCH_3), 3.88 (s, 6H, 3,5-MetaArOCH_3). HRMS (ESI, TOF) m/z calcd for C$_{22}$H$_{20}$BO$_5$F$_2$: 413.1372 [M + H]$^+$; found 413.1379.

RESULTS and DISCUSSION

Synthesis. Boron dye derivatives **1-5** were prepared as previously described in two steps (Scheme 1).[22] Briefly, β–diketone ligands were prepared by Claisen condensation between an aromatic ketone and an aromatic ester in the presence of NaH. Ligands dissolved readily in common organic solvents (acetone, EtOAc, CH$_2$Cl$_2$) and were purified by recrystallization from acetone/hexanes. The corresponding boron complexes were prepared in methylene chloride by addition of boron trifluoride diethyl etherate. Boron complexes **1**, **2** and **4** showed high solubility in common organic solvents (e.g. acetone, CH$_2$Cl$_2$), whereas the naphthalene derivatives **3** and **5** showed more limited solubility in solvents such as acetone. All dyes were purified by recrystallization from acetone/hexanes. These rapid, column-free syntheses are promising for lowering the cost and increasing the convenience of producing dual-emissive materials.

Scheme 1. Representative synthesis of BF$_2$bdks

Optical Properties in CH₂Cl₂ Solution. Boron dyes **1-5** were studied in dilute CH_2Cl_2 solution for ready comparison of optical properties with those corresponding to other BF_2bdk dyes previously reported by our group.[14,22,83] Data are summarized in Table 1. The optical properties of compound **1** are in good agreement with a previous report by Sket et al.[75]

Table 1. Optical Properties of Boron Dyes in CH_2Cl_2 (λ_{ex} = 369 nm)

BF₂bdk	$\lambda_{abs}{}^a$ (nm)	ε^b (M⁻¹ cm⁻¹)	$\lambda_F{}^c$ (nm)	$\tau_F{}^d$ (ns)	Φ^e	$\tau_{rad}{}^f$ (ns)	$k_r{}^g$ (ns⁻¹)	$k_{nr}{}^h$ (ns⁻¹)
1	369	33 200	554	6.87	0.05	137.4	<0.01	0.14
2	396	47 300	525	7.40	0.08	92.5	0.01	0.12
3	402	35 200	560	4.84	0.05	96.8	0.01	0.20
4	391	44 600	567	4.53	0.04	113.4	<0.01	0.21
5	427	50 000	520	4.32	0.95	4.5	0.22	0.01

a. Absorbance maxima
b. Extinction coefficient
c. Fluorescence maxima
d. Fluorescence lifetime
e. Fluorescence quantum yield versus quinine sulfate in 0.1 M H_2SO_4.[84]
f. Radiative lifetime: $\tau_{rad} = \tau_F/\Phi_F$[22]
g. Radiative rate constant: $k_r = \Phi_F/\tau_F$[85]
h. Non-radiative rate constant: $k_{nr} = (1-\Phi_F)/\tau_F$[85]

Dyes **1-4** showed ultraviolet absorption (369-402 nm) in CH_2Cl_2, while compound **5** showed more red-shifted absorption (427 nm; Figure S1). The emission wavelength in CH_2Cl_2 showed no distinct trend amongst the derivatives with regard to π–conjugation. Compound **4**, the thienyl derivative, showed the most red-shifted emission in CH_2Cl_2 solution (567 nm); whereas,

compound **5**, with the greatest π–conjugation across the molecule, exhibited the most blue-shifted emission (520 nm).

All the dyes displayed long fluorescence lifetimes (4-7 ns) compared to *para*-substituted derivatives (~2 ns), but varying quantum yields. The quantum yield of dyes **1-4** in solution were very low (Φ_F = 0.04-0.08), while compound **5** showed highly efficient emission (Φ_F = 0.95). Calculations of the radiative (k_r) and non-radiative (k_{nr}) rate constants support these results (Table 1). Dyes with low quantum yields have rapid rates of non-radiative decay, corroborating ICT transitions.[86–88] Dyes with ICT character (**1-4**) have faster rates of fluorescence deactivation (i.e. non-radiative decay; k_{nr} = 0.12 − 0.21 ns^{-1}) than of radiative decay (k_r ≤ 0.01 ns^{-1}). In contrast, compound **5** with less ICT character, showed the opposite trend with the radiative rate more rapid than the non-radiative rate (k_{nr} = 0.01 and k_r = 0.22). The radiative lifetimes (τ_{rad}) support these results.[52] This measurement, also known as the intrinsic lifetime, is the fluorescence lifetime in the absence of non-radiative decay pathways. In previous reports of BF$_2$bdks, τ_{rad} values around 10 ns were indicative of intramolecular charge transfer (ICT), whereas lower τ_{rad} values around 2 ns were ascribed to π–π∗ transitions.[22] The τ_{rad} values of compounds **1-4** are 100-150 ns, whereas compound **5**, showed the shortest radiative lifetime (4.53 ns). This clearly revealed that compounds **1-4** have dramatically stronger ICT properties compared to compound **5**. To further confirm this, solvatochromism experiments and density-functional theory computational studies were performed.

Solvatochromism. All the dyes exhibited long fluorescence lifetimes (> 4 ns), and therefore, the emission is expected to be very sensitive to solvent polarity.[89] The solvatochromic behaviors of dyes **1-5** were investigated in solvents of variable polarity, but similar viscosity to eliminate other (e.g. viscochromic) influences (Figures 2, S2-S3). Hexane, toluene, methylene

chloride, acetone, and acetonitrile were selected. Using Lippert-Mataga theory, the Stokes shift (Δv) was plotted versus the solvent polarity parameter (Δf) (Figure S4).[76] In non-polar solvents, such as hexanes, dyes **1-4** showed violet fluorescence at around 400 nm, except for **5**, which showed blue fluorescence at 430 nm. With increasing polarity, the emission of dyes **1-4** redshifted dramatically, and the fluorescence intensities sharply decreased, to where the dyes are virtually non-emissive. In comparison, the fluorescence of compound **5** red-shifted with increasing polarity, but for this dye the signal remained bright. The slope of the Lippert-Mataga plots showed that compound **2** had the strongest solvatochromic behavior, while compounds **3** and **5** showed the weakest response to polarity (Lippert-Mataga slope; **3** = 19.8, **5** = 12.6) (Figure S4). In more polar solvents, the longer wavelength emission may be influenced by the rate of intersystem crossing as well.[90] Stabilization of the fluorescence at a lower energy, closer to the triplet state, enhances the rate of intersystem crossing.[91] In polar organic solvents, the energy is readily dissipated non-radiatively (e.g. low quantum yield; Table S1). However, compound **5** did not display the same dramatic decrease in emission intensity exhibited by compounds **1-4**. Therefore, this scaffold likely has different electronic properties, and could be more useful as a solvatochromic dye sensor.[89]
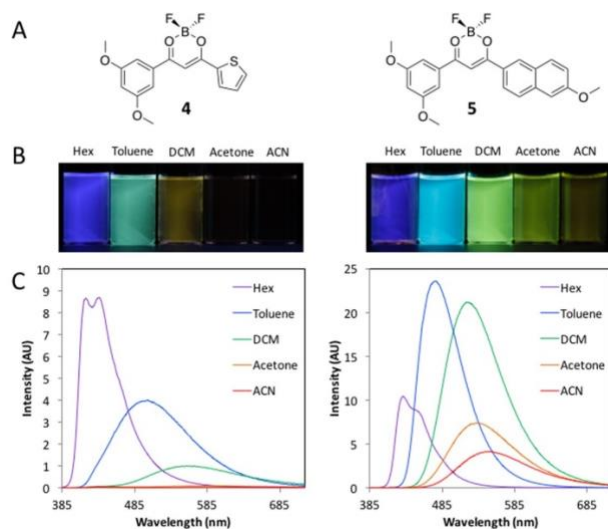
Figure 2. Solvent-Sensitive Emission of Charge Transfer Boron Complexes (λ_{ex} = 369 nm for images and spectra). A) Representative dyes (note: behavior of **1**, **2** and **3** are like **4**). B) Images of the dyes in various solvents (left to right; n-hexanes (Hex), toluene, dichloromethane (DCM), acetone, and acetonitrile (ACN) C) Total emission spectra in various solvents (left to right; n-hexanes (Hex), toluene, dichloromethane (DCM), acetone, and acetonitrile (ACN).

Computational Studies. Computational study of the qualitative molecular orbitals (MOs) provided insight into the ICT behaviors of the dyes (Figure 3; Supporting Information). Ground state geometries and energies of the singlet ground state (S_0) are reported for dyes **1-5**. All the dyes showed highly planar structures, important for producing red-shifted phosphorescence and reducing twisted intramolecular charge transfer (TICT).[22] The qualitative MOs of compounds **1-4** are nearly identical in character. In the highest occupied molecular orbital (HOMO), electron density is localized on the 3,5-dimethoxy aromatic, and in the lowest unoccupied molecular orbital (LUMO), electron density is delocalized across the entire molecule. This is indicative of ICT behavior, as areas devoid of electron density in the HOMO (e.g. phenyl in **2**, thienyl in **4**), become electron dense in the LUMO (Figure 3 and Tables S2-S6).[92] The π–localized HOMO to $\pi*$–delocalized LUMO is a common transition for solvatochromic fluorophores. However, calculated absorption spectra show the main transition during excitation is the HOMO-1 to LUMO (Tables S1-S5). The HOMO-1 (or HOMO-2 for compound **3**) to LUMO is π–$\pi*$ for compounds

1-4, whereas the ICT transition (HOMO-LUMO) is expressed as a weaker, lower energy transition. In contrast, MO diagrams of compound **5** showed delocalized HOMO and LUMO electron density, indicative of a π–π* transition (Figure 3).[22] This explains the anomalous behavior of compound **5** in comparison to dyes **1-4**, such as bright emission and short radiative lifetime. The qualitative MOs, in combination with the solvatochromism experiments indicate molecules with strong (**1-4**) or moderate (**5**) charge transfer.
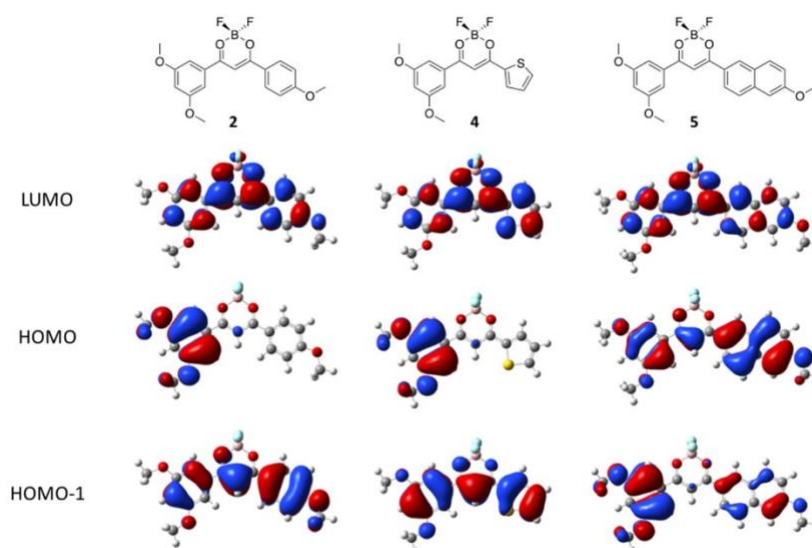

Figure 3. Frontier molecular orbitals of compounds **2**, **4**, and **5**. (Compounds **1** and **3** are similar to **2** and are shown in Tables S1-S5).

Luminescence in PLA Blends. To observe the phosphorescence properties, dilute dye/PLA blends (1% weight percent) were generated by co-dissolution of the dye and the polymer in a minimal amount of CH_2Cl_2, and slow evaporation of the solvent to make a film of the mixture on the inside wall of a glass vial (Figure S6). The vial is a convenient chamber for controlling the oxygen environment. At low dye loading (1 wt%), there is a low propensity for the dyes to aggregate,[58] which corresponds to the largest gaps between the fluorescence and phosphorescence peaks,[59] and increased photostability of the oxygen-sensing material.[66] The optical properties are

presented in Table 2, namely, fluorescence wavelengths (λ_F) and lifetimes (τ_F), phosphorescence wavelengths (λ_{RTP}) and lifetimes (τ_{RTP}), and the F/P ratios. Important considerations for ratiometric oxygen sensing include emission color[93] and the gap between fluorescence and phosphorescence.[94] For bioimaging, red-emitting dyes are used for deeper tissue imaging because of benefits in decreased light scattering.[95,96] However, for other applications, such as industrial sensors, red-emitting dyes are not essential; rather, distinguishable singlet and triplet emissions and readily detectable emission intensity are priorities.[67,97]

Table 2. Optical Properties of Boron Dyes in PLA[a]

BF$_2$bdk	$\lambda_F{}^{b}$ (nm)	$\tau_F{}^{c}$ (ns)	$\lambda_{RTP}{}^{d}$ (nm)	$\tau_{RTP}{}^{e}$ (ms)	F/P[f]
1	487	8.44	523	213	0.48
2	449	3.71	521	274	1.18
3	469	5.13	545	447	0.86
4	470	4.80	560	154	0.43
5	491	4.85	533	181	NA[g]

a. 1.0 weight percent dye in PLA (λ_{ex} = 369 nm)
b. Fluorescence maxima
c. Fluorescence lifetime
d. Delayed emission maxima under N_2 (1 ms delay time)
e. Phosphorescence lifetime under N_2, monitored at the delayed emission maxima
f. Ratio of fluorescence to phosphorescence under N_2
g. Fluorescence and phosphorescence peaks are too close to assign distinct peaks under N_2.

The fluorescence properties of the films were analyzed in air at room temperature. Under these conditions, phosphorescence is quenched. In the PLA blends, all the dyes showed blue to green fluorescence (449 - 491 nm). Compound **2** showed the most blue-shifted fluorescence, while compound **5** showed the most redshifted emission. The fluorescence wavelength can be linked to different factors, such as π−conjugation and ICT, though trends are sometimes difficult to rationalize. For example, compound **1**, with a simple structure and a lower degree of π−conjugation (phenyl), showed more red-shifted fluorescence (λ_F = 487 nm) than compound **3** (naphthyl; λ_F =

470 nm). Charge transfer may play a more important role than the π–conjugation in determining emission color.[98]

To analyze the phosphorescence properties, the films in vials were fitted with Teflon sealed caps and a vent needle and were continuously purged with N_2 during the measurements. All dyes showed delayed emission under N_2 (i.e. phosphorescence or thermally-activated delayed fluorescence; Figure S7). The phosphorescence wavelengths were highly dependent on aromatic substitution. The phenyl derivatives (**1** and **2**) showed green phosphorescence (~520 nm), the naphthyl derivative (**3**), yellow phosphorescence (545 nm), and the thienyl dye (**4**), yellow-orange phosphorescence (560 nm). The color tunability of the phosphorescence is an important feature for multiplexing bioimaging.[99,100]

The relative fluorescence to phosphorescence intensity (F/P) for the 3,5-dimethoxy dyes is noteworthy. Strong phosphorescence is observed for heavy-atom free fluorophores (Figure 4). For compound **1**, the total emission intensity increased twofold under N_2, with separated fluorescence and phosphorescence. This difluoroboron dibenzolymethane (BF$_2$dbm) derivative (compound **1**) can be compared to other alkoxy-substituted dyes in a previous report by Daly et al.[74] As seen in Figure S8, the charge-transfer properties, linked to the solvatochromic behavior, are highly modular based on the alkoxy-substitution pattern. In the previous study, by altering the position of a single alkoxy group from the *para-* to the *meta-* position of an aromatic ring (*para-*BF$_2$dbmOC$_{12}$H$_{25}$ vs *meta-*BF$_2$dbmOC$_{12}$H$_{25}$), the charge transfer property is greatly enhanced, indicated by red-shifted fluorescence [101] (λ_F: para, 432 nm; meta, 459 nm), a longer-lived fluorescence lifetime[102] (τ_F: para, 3.59; meta, 5.49 ns), and enhanced phosphorescence to fluorescence ratio under N_2[62] (F/P: para, 4.9; meta, 1.2. Note: smaller F/P = more intense phosphorescence) when embedded in PLA. In this study, methoxy substituents at both *meta*

positions takes this effect one step further. For compound **1**, charge transfer increases more dramatic in the PLA matrix (λ_F = 487 nm, τ_F = 8.44 ns, F/P = 0.5), resulting in a material with phosphorescence twice as strong as the fluorescence (Figure 4 and Table S2). Among the three dyes, namely the mono-substituted para and meta dyes in the previous study and compound **1** here, the fluorescence steadily red-shifted with increasing charge-transfer characteristics (432 nm, 459 nm and 487 nm), while the phosphorescence is relatively static (525 nm ±10). Therefore, the increase in phosphorescence may be primarily attributed to the decrease in the singlet-triplet gap (Δ_{F-P}), leading to an accelerated rate of intersystem crossing (ISC) (Table S2).[103–105] This is further supported by consideration of optical properties of compound **2**. Relative to **1**, compound **2** has blue-shifted fluorescence (λ_F; **1** = 487 nm, **2** = 447 nm) and a larger singlet-triplet gap (Δ_{F-P}: **1** = 36 nm, **2** = 72 nm). This resulted in compound **2** having weaker phosphorescence intensity (Figure 4).

Upon changing the atmosphere from air to N_2, compounds **2-4** revealed phosphorescence as a second peak of equal or stronger intensity than the fluorescence. *This is highly unusual for heavy-atom free phosphorescent materials with methoxy groups on the para position of the aromatic ring, for which the phosphorescence can typically only be observed by time-resolved methods (e.g. delayed emission spectra).*[22,23,49] In particular, compound **4**, showed the strongest phosphorescence with the largest fluorescence to phosphorescence gap, ideal for red/green/blue (RGB) camera channel imaging.[44] Furthermore, because there is no heavy atom, the lifetimes are ultralong—a feature that is not seen with heavy-atom substitution (Figure 5).[49,67] A material like dye **4** in PLA can be used as a multimodal trace oxygen sensor (i.e. lifetime or ratiometry).[44] Compound **5** did not show discrete fluorescence and phosphorescence peaks under N_2 (Figure S9).

Therefore, the strong charge-transfer character of compounds **1-4** may be the key feature in creating the strong phosphorescence in these systems.
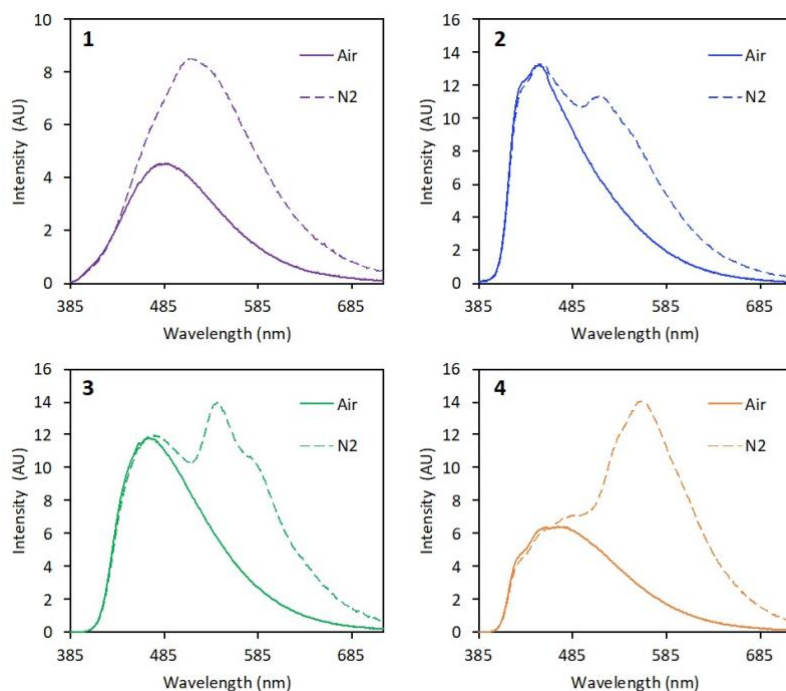

Figure 4. Total emission spectra of dual emissive dyes **1-4** in PLA fabricated as films in vials under air and nitrogen (N_2).
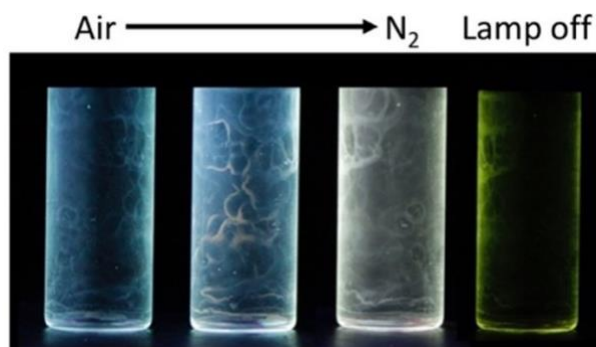

Figure 5. Phosphorescence properties of compound **4** in PLA (1% dye in PLA; weight percent). Images are time lapse snapshots of dye/polymer films sealed in vials and purged with nitrogen overtime. From left to right, purge time = 0 s (far left), 30 s (middle left), and 1min (middle right), then after the UV lamp was turned off to observe the phosphorescence afterglow (far right) (λ_{ex} = 369 nm).

CONCLUSION

The synthesis and optical properties of *meta*-dimethoxy difluoroboron β–diketonates in PLA with intensified phosphorescence were described. By introducing two methoxy groups at the *meta* positions, the charge-transfer character of the fluorophores is enhanced versus the more commonly studied *para* position substitution. Solvatochromic behavior and computational results showed these dyes have localized HOMO orbitals and delocalized LUMO orbitals, indicative of strong charge transfer character. When the dyes are embedded into a rigid matrix, such as PLA, the charge transfer character of the dyes promoted increased intersystem crossing and enhanced phosphorescence. This feature made the dyes unique as heavy-atom free materials with intensified phosphorescence and ultralong phosphorescence lifetimes (100-400 ms). In particular, compound **4**, the thienyl derivative, has phosphorescence twice as strong as the fluorescence. While initial tests of the dyes **2-5** showed no remarkable solid-state properties, such as the mechanochromism seen for **1**, in polymers these dyes show promise for trace oxygen sensors with multimodal imaging capabilities via lifetime or ratiometric techniques.

ASSOCIATED CONTENT

The following files are available free of charge.

Synthesis scheme, UV-vis in CH_2Cl_2, solvatochromism data, phosphorescence data, ^1H NMR and computational data.

AUTHOR INFORMATION

Corresponding Author

*Cassandra L. Fraser: fraser@virginia.edu

Present Addresses

†Satoru Hiroto: Graduate School of Human and Environmental Studies, Kyoto University, Sakyo-ku, Kyoto, 606-8501, Japan

Author Contributions

The manuscript was written through contributions of all authors. All authors have given approval to the final version of the manuscript.

REFERENCES

(1)   Wolfbeis, O. S. An Overview of Nanoparticles Commonly Used in Fluorescent Bioimaging. *Chem. Soc. Rev.* **2015**, *44*, 4743–4768.

(2)   Lavis, L. D.; Raines, R. T. Bright Building Blocks for Chemical Biology. *ACS Chem. Biol.* **2014**, *9*, 855–866.

(3)   Aron, A. T.; Ramos-Torres, K. M.; Cotruvo, J. A.; Chang, C. J. Recognition- and Reactivity-Based Fluorescent Probes for Studying Transition Metal Signaling in Living Systems. *Acc. Chem. Res.* **2015**, *48*, 2434–2442.

(4)   Chan, J.; Dodani, S. C.; Chang, C. J. Reaction-Based Small-Molecule Fluorescent Probes for Chemoselective Bioimaging. *Nat. Chem.* **2012**, *4*, 973–984.

(5)   Li, D.; Zhang, H.; Wang, Y. Four-Coordinate Organoboron Compounds for Organic Light-Emitting Diodes (OLEDs). *Chem. Soc. Rev.* **2013**, *42*, 8416–8433.

(6)   Bagher, A. M. OLED Display Technology. *Am. J. Opt. Photonics* **2014**, *2*, 32–36.

(7)   Siraj, N.; El-Zahab, B.; Hamdan, S.; Karam, T. E.; Haber, L. H.; Li, M.; Fakayode, S. O.; Das, S.; Valle, B.; Strongin, R. M.; et al. Fluorescence, Phosphorescence, and Chemiluminescence. *Anal. Chem.* **2016**, *88*, 170–202.

(8)   Grimm, J. B.; English, B. P.; Chen, J.; Slaughter, J. P.; Zhang, Z.; Revyakin, A.; Patel, R.; Macklin, J. J.; Normanno, D.; Singer, R. H.; et al. A General Method to Improve Fluorophores for Live-Cell and Single-Molecule Microscopy. *Nat. Methods* **2015**, *12*, 244–250.

(9)   Lavis, L. D.; Raines, R. T. Bright Ideas for Chemical Biology. *ACS Chem. Biol.* **2008**, *3*, 142–155.

(10)   Wang, J. X.; Niu, L. Y.; Chen, P. Z.; Chen, Y. Z.; Yang, Q. Z.; Boulatov, R. Ratiometric O2 Sensing Based on Selective Self-Sensitized Photooxidation of Donor-Acceptor Fluorophores. *Chem. Commun.* **2019**, *55*, 7017–7020.

(11)   Karpenko, I. A.; Niko, Y.; Yakubovskyi, V. P.; Gerasov, A. O.; Bonnet, D.; Kovtun, Y. P.; Klymchenko, A. S. Push–Pull Dioxaborine as Fluorescent Molecular Rotor: Far-Red Fluorogenic Probe for Ligand–Receptor Interactions. *J. Mater. Chem. C* **2016**, *4*, 3002–3009.

(12)   Yang, Y.; Hughes, R. P.; Aprahamian, I. Visible Light Switching of a BF $_2$ -Coordinated Azo Compound. *J. Am. Chem. Soc.* **2012**, *134*, 15221–15224.

(13)   Kubota, Y.; Sakuma, Y.; Funabiki, K.; Matsui, M. Solvatochromic Fluorescence Properties of Pyrazine–Boron Complex Bearing a β-Iminoenolate Ligand. *J. Phys. Chem. A* **2014**, *118*, 8717–8729.

(14)   Butler, T.; Morris, W. A.; Samonina-Kosicka, J.; Fraser, C. L. Mechanochromic Luminescence and Aggregation Induced Emission of Dinaphthoylmethane β-Diketones and Their Boronated Counterparts. *ACS Appl. Mater. Interfaces* **2016**, *8*, 1242–1251.

(15)   Tanaka, K.; Chujo, Y. Recent Progress of Optical Functional Nanomaterials Based on Organoboron Complexes with β-Diketonate, Ketoiminate and Diiminate. *NPG Asia Mater.* **2015**, *7*, e223.

(16) Chen, P. Z.; Niu, L. Y.; Chen, Y. Z.; Yang, Q. Z. Difluoroboron β-Diketonate Dyes: Spectroscopic Properties and Applications. *Coord. Chem. Rev.* **2017**, *350*, 196–216.

(17) DeRosa, C. A.; Fraser, C. L. Tetracoordinate Boron Materials for Biological Imaging. In *Main Group Strategies towards Functional Hybrid Materials*; John Wiley & Sons, Ltd: Chichester, UK, 2018; pp 111–140.

(18) Yin, X.; Chen, J.; Lalancette, R. A.; Marder, T. B.; Jäkle, F. Highly Electron-Deficient and Air-Stable Conjugated Thienylboranes. *Angew. Chem. Int. Ed..* **2014**, *53*, 9761–9765.

(19) Yin, X.; Guo, F.; Lalancette, R. A.; Jäkle, F. Luminescent Main-Chain Organoborane Polymers: Highly Robust, Electron-Deficient Poly(Oligothiophene Borane)s via Stille Coupling Polymerization. *Macromolecules* **2016**, *49*, 537–546.

(20) Jäkle, F. Advances in the Synthesis of Organoborane Polymers for Optical, Electronic, and Sensory Applications. *Chem. Rev.* **2010**, *110*, 3985–4022.

(21) Daly, M. L.; DeRosa, C. A.; Kerr, C.; Morris, W. A.; Fraser, C. L. Blue Thermally Activated Delayed Fluorescence from a Biphenyl Difluoroboron β-Diketonate. *RSC Adv.* **2016**, *6*, 81631–81635.

(22) Xu, S.; Evans, R. E.; Liu, T.; Zhang, G.; Demas, J. N.; Trindle, C. O.; Fraser, C. L. Aromatic Difluoroboron β-Diketonate Complexes: Effects of π-Conjugation and Media on Optical Properties. *Inorg. Chem.* **2013**, *52*, 3597–3610.

(23) Zhang, G.; Chen, J.; Payne, S. J.; Kooi, S. E.; Demas, J. N.; Fraser, C. L. Multi-Emissive Difluoroboron Dibenzoylmethane Polylactide Exhibiting Intense Fluorescence and Oxygen-Sensitive Room-Temperature Phosphorescence. *J. Am. Chem. Soc.* **2007**, *129*, 8942–8943.

(24) Madhavan Nampoothiri, K.; Nair, N. R.; John, R. P. An Overview of the Recent Developments in Polylactide (PLA) Research. *Bioresour. Technol.* **2010**, *101*, 8493–8501.

(25) Farah, S.; Anderson, D. G. Physical and Mechanical Properties of PLA, and Their Functions in Widespread Applications — A Comprehensive Review. *Adv. Drug Deliv. Rev.* **2016**,

107, 367–392.

(26) Kerr, C.; DeRosa, C. A.; Daly, M. L.; Zhang, H.; Palmer, G. M.; Fraser, C. L. Luminescent Difluoroboron β-Diketonate PLA–PEG Nanoparticles. *Biomacromolecules* **2017**, *18*, 551–561.

(27) Kersey, F. R.; Zhang, G.; Palmer, G. M.; Dewhirst, M. W.; Fraser, C. L. Stereocomplexed Poly(Lactic Acid)-Poly(Ethylene Glycol) Nanoparticles with Dual-Emissive Boron Dyes for Tumor Accumulation. *ACS Nano* **2010**, *4*, 4989–4996.

(28) Yang, Z.; Mao, Z.; Xie, Z.; Zhang, Y.; Liu, S.; Zhao, J.; Xu, J.; Chi, Z.; Aldred, M. P. Recent Advances in Organic Thermally Activated Delayed Fluorescence Materials. *Chem. Soc. Rev.* **2017**, *46*, 915–1016.

(29) Koch, M.; Perumal, K.; Blacque, O.; Garg, J. A.; Saiganesh, R.; Kabilan, S.; Balasubramanian, K. K.; Venkatesan, K. Metal-Free Triplet Phosphors with High Emission Efficiency and High Tunability. *Angew. Chem. Int. Ed.* **2014**, *53*, 6378–6382.

(30) Xiang, H.; Cheng, J.; Ma, X.; Zhou, X.; Chruma, J. J. Near-Infrared Phosphorescence: Materials and Applications. *Chem. Soc. Rev.* **2013**, *42*, 6128–6185.

(31) Gupta, S. K.; Haridas, A.; Choudhury, J. Remote Terpyridine Integrated NHC – Ir III Luminophores as Potential Dual-Emissive Ratiometric O 2 Probes. *Chem. - A Eur. J.* **2017**, *23*, 4770–4773.

(32) Baggaley, E.; Gill, M. R.; Green, N. H.; Turton, D.; Sazanovich, I. V.; Botchway, S. W.; Smythe, C.; Haycock, J. W.; Weinstein, J. A.; Thomas, J. A. Dinuclear Ruthenium(II) Complexes as Two-Photon, Time-Resolved Emission Microscopy Probes for Cellular DNA. *Angew. Chem. Int. Ed.* **2014**, *53*, 3367–3371.

(33) Baggaley, E.; Weinstein, J. A.; Williams, J. A. G. Time-Resolved Emission Imaging Microscopy Using Phosphorescent Metal Complexes: Taking FLIM and PLIM to New Lengths; Springer Berlin Heidelberg, 2014; pp 205–256.

(34) An, Z.; Zheng, C.; Tao, Y.; Chen, R.; Shi, H.; Chen, T.; Wang, Z.; Li, H.; Deng, R.; Liu,

X.; et al. Stabilizing Triplet Excited States for Ultralong Organic Phosphorescence. *Nat. Mater.* **2015**, *14*, 685–690.

(35)   Zhen, X.; Tao, Y.; An, Z.; Chen, P.; Xu, C.; Chen, R.; Huang, W.; Pu, K. Ultralong Phosphorescence of Water-Soluble Organic Nanoparticles for In Vivo Afterglow Imaging. *Adv. Mater.* **2017**, *29*, 1606665.

(36)   Xu, S.; Chen, R.; Zheng, C.; Huang, W. Excited State Modulation for Organic Afterglow: Materials and Applications. *Adv. Mater.* **2016**, *28*, 9920–9940.

(37)   Wang, X.; Stolwijk, J. A.; Lang, T.; Sperber, M.; Meier, R. J.; Wegener, J.; Wolfbeis, O. S. Ultra-Small, Highly Stable, and Sensitive Dual Nanosensors for Imaging Intracellular Oxygen and PH in Cytosol. *J. Am. Chem. Soc.* **2012**, *134*, 17011–17014.

(38)   Feng, Y.; Cheng, J.; Zhou, L.; Zhou, X.; Xiang, H. Ratiometric Optical Oxygen Sensing: A Review in Respect of Material Design. *Analyst* **2012**, *137*, 4885–4901.

(39)   Roussakis, E.; Li, Z.; Nichols, A. J.; Evans, C. L. Oxygen-Sensing Methods in Biomedicine from the Macroscale to the Microscale. *Angew. Chemie Int. Ed.* **2015**, *54*, 8340–8362.

(40)   Quaranta, M.; Borisov, S. M.; Klimant, I. Indicators for Optical Oxygen Sensors. *Bioanal. Rev.* **2012**, *4* 115–157.

(41)   Wang, X.; Wolfbeis, O. S. Optical Methods for Sensing and Imaging Oxygen: Materials, Spectroscopies and Applications. *Chem. Soc. Rev.* **2014**, *43*, 3666–3761.

(42)   Dmitriev, R. I.; Borisov, S. M.; Kondrashina, A. V.; Pakan, J. M. P.; Anilkumar, U.; Prehn, J. H. M.; Zhdanov, A. V.; McDermott, K. W.; Klimant, I.; Papkovsky, D. B. Imaging Oxygen in Neural Cell and Tissue Models by Means of Anionic Cell-Permeable Phosphorescent Nanoparticles. *Cell. Mol. Life Sci.* **2015**,*72*, 367–381.

(43)   Dmitriev, R. I.; Borisov, S. M.; Du, H.; Düssmann, H.; Sun, S.; Müller, B. J.; Prehn, J.; Baklaushev, V. P.; Klimant, I.; Papkovsky, D. B. Versatile Conjugated Polymer Nanoparticles for High-Resolution O2 Imaging in Cells and 3D Tissue Models. *ACS Nano* **2015**, *9*, 5275–5288.

(44)   DeRosa, C. A.; Seaman, S. A.; Mathew, A. S.; Gorick, C. M.; Fan, Z.; Demas, J. N.; Peirce, S. M.; Fraser, C. L. Oxygen Sensing Difluoroboron B−Diketonate Polylactide Materials with Tunable Dynamic Ranges for Wound Imaging. *ACS Sens.* **2016**, *1*, 1366–1373.

(45)   Li, X.; Liu, H.; Sun, X.; Bi, G.; Zhang, G. Highly Fluorescent Dye-Aggregate-Enhanced Energy-Transfer Nanoparticles for Neuronal Cell Imaging. *Adv. Opt. Mater.* **2013**, *1* 549–553.

(46)   Wang, X.-H.; Peng, H.-S.; Ding, H.; You, F.-T.; Huang, S.-H.; Teng, F.; Dong, B.; Song, H.-W. Biocompatible Fluorescent Core–Shell Nanoparticles for Ratiometric Oxygen Sensing. *J. Mater. Chem.* **2012**, *22*, 16066–16071.

(47)   Lu, S.; Xu, W.; Zhang, J.; Chen, Y.; Xie, L.; Yao, Q.; Jiang, Y.; Wang, Y.; Chen, X. Facile Synthesis of a Ratiometric Oxygen Nanosensor for Cellular Imaging. *Biosens. Bioelectron.* **2016**, *86*, 176–184.

(48)   Payne, S. J.; Zhang, G.; Demas, J. N.; Fraser, C. L.; Degraff, B. A. Laser Phosphoroscope and Applications to Room-Temperature Phosphorescence. *Appl. Spectrosc.* **2011**, *65*, 1321–1324.

(49)   Mathew, A. S.; DeRosa, C. A.; Demas, J. N.; Fraser, C. L. Difluoroboron β-Diketonate Materials with Long-Lived Phosphorescence Enable Lifetime Based Oxygen Imaging with a Portable Cost Effective Camera. *Anal. Methods* **2016**, *8*, 3109–3114.

(50)   Hirata, S.; Vacha, M. Circularly Polarized Persistent Room-Temperature Phosphorescence from Metal-Free Chiral Aromatics in Air. *J. Phys. Chem. Lett.* **2016**, *7*, 1539–1545.

(51)   Hirata, S.; Vacha, M. White Afterglow Room-Temperature Emission from an Isolated Single Aromatic Unit under Ambient Condition. *Adv. Opt. Mater.* **2017**, 1600996.

(52)   Lower, S. K.; El-Sayed, M. A. The Triplet State and Molecular Electronic Processes in Organic Molecules. *Chem. Rev.* **1966**, *66*, 199–241.

(53)   Ferree, W. I.; Plummer, B. F. Internal Heavy-Atom Effects upon the Reaction of Acenaphthylene with Cyclopentadiene. **1972**, *306*, 6709–6717.

(54)   Tanielian, C.; Wolff, C. Determination of the Parameters Controlling Singlet Oxygen Production via Oxygen and Heavy-Atom Enhancement of Triplet Yields1. **1995**, 99, 9831–9837.

(55)   Mukherjee, S.; Thilagar, P. Recent Advances in Purely Organic Phosphorescent Materials. *Chem. Commun.* **2015**, *51*, 10988–11003.

(56)   Morris, W. A.; Liu, T.; Fraser, C. L. Mechanochromic Luminescence of Halide-Substituted Difluoroboron β-Diketonate Dyes. *J. Mater. Chem. C* **2015**, *3*, 352-363.

(57)   Morris, W. A.; Sabat, M.; Butler, T.; DeRosa, C. A.; Fraser, C. L. Modulating Mechanochromic Luminescence Quenching of Alkylated Iodo Difluoroboron Dibenzoylmethane Materials. *J. Phys. Chem. C* **2016**, *120*, 14289–14300.

(58)   DeRosa, C. A.; Samonina-Kosicka, J.; Fan, Z.; Hendargo, H. C.; Weitzel, D. H.; Palmer, G. M.; Fraser, C. L. Oxygen Sensing Difluoroboron Dinaphthoylmethane Polylactide. *Macromolecules* **2015**, *48*, 2967–2977.

(59)   Zhang, G.; Palmer, G. M.; Dewhirst, M. W.; Fraser, C. L. A Dual-Emissive-Materials Design Concept Enables Tumour Hypoxia Imaging. *Nat. Mater.* **2009**, *8*, 747–751.

(60)   Gutierrez, G. D.; Sazama, G. T.; Wu, T.; Baldo, M. A.; Swager, T. M. Red Phosphorescence from Benzo[2,1,3]Thiadiazoles at Room Temperature. *J. Org. Chem.* **2016**, *81*, 4789–4796.

(61)   Ventura, B.; Bertocco, A.; Braga, D.; Catalano, L.; D'Agostino, S.; Grepioni, F.; Taddei, P. Luminescence Properties of 1,8-Naphthalimide Derivatives in Solution, in Their Crystals, and in Co-Crystals: Toward Room-Temperature Phosphorescence from Organic Materials. *J. Phys. Chem. C* **2014**, *118*, 18646–18658.

(62)   Chen, X.; Xu, C.; Wang, T.; Zhou, C.; Du, J.; Wang, Z.; Xu, H.; Xie, T.; Bi, G.; Jiang, J.; et al. Versatile Room-Temperature-Phosphorescent Materials Prepared from N-Substituted Naphthalimides: Emission Enhancement and Chemical Conjugation. *Angew. Chem. Int. Ed.* **2016**, *55*, 9872–9876.

(63)   Guo, S.; Wu, W.; Guo, H.; Zhao, J. Room-Temperature Long-Lived Triplet Excited States

of Naphthalenediimides and Their Applications as Organic Triplet Photosensitizers for Photooxidation and Triplet-Triplet Annihilation Upconversions. *J. Org. Chem.* **2012**, *77*, 3393–3943.

(64) Yu, Y.; Kwon, M. S.; Jung, J.; Zeng, Y.; Kim, M.; Chung, K.; Gierschner, J.; Youk, J. H.; Borisov, S. M.; Kim, J. Room-Temperature-Phosphorescence-Based Dissolved Oxygen Detection by Core-Shell Polymer Nanoparticles Containing Metal-Free Organic Phosphors. *Angew. Chem. Int. Ed.* **2017**, *56*, 16207–16211.

(65) Bolton, O.; Lee, K.; Kim, H.-J.; Lin, K. Y.; Kim, J. Activating Efficient Phosphorescence from Purely Organic Materials by Crystal Design. *Nat. Chem.* **2011**, *3*, 205–210.

(66) DeRosa, C. A.; Kerr, C.; Fan, Z.; Kolpaczynska, M.; Mathew, A. S.; Evans, R. E.; Zhang, G.; Fraser, C. L. C. L. Tailoring Oxygen Sensitivity with Halide Substitution in Difluoroboron Dibenzoylmethane Polylactide Materials. *ACS Appl. Mater. Interfaces* **2015**, *7*, 23633–23643.

(67) Lehner, P.; Staudinger, C.; Borisov, S. M.; Klimant, I. Ultra-Sensitive Optical Oxygen Sensors for Characterization of Nearly Anoxic Systems. *Nat. Commun.* **2014**, *5*, 4460.

(68) Lehner, P.; Staudinger, C.; Borisov, S. M.; Regensburger, J.; Klimant, I. Intrinsic Artefacts in Optical Oxygen Sensors--How Reliable Are Our Measurements? *Chem. - A Eur. J.* **2015**, *21*, 3978–3986.

(69) Zhang, G.; Evans, R. E.; Campbell, K. a.; Fraser, C. L. Role of Boron in the Polymer Chemistry and Photophysical Properties of Difluoroboron-Dibenzoylmethane Polylactide. *Macromolecules* **2009**, *42*, 8627–8633.

(70) Zhang, X.; Xie, T.; Cui, M.; Yang, L.; Sun, X.; Jiang, J.; Zhang, G. General Design Strategy for Aromatic Ketone-Based Single-Component Dual-Emissive Materials. *ACS Appl. Mater. Interfaces* **2014**, *6*, 2279–2284.

(71) Grätzel, M. Dye-Sensitized Solar Cells. *J. Photochem. Photobiol. C Photochem. Rev.* **2003**, *4* (2), 145–153.

(72)   Samonina-Kosicka, J.; DeRosa, C. A.; Morris, W. A.; Fan, Z.; Fraser, C. L. Dual-Emissive Difluoroboron Naphthyl-Phenyl β-Diketonate Polylactide Materials: Effects of Heavy Atom Placement and Polymer Molecular Weight. *Macromolecules* **2014**, *47*, 3736–3746.

(73)   Liu, T.; Zhang, G.; Evans, R. E.; Trindle, C. O.; Altun, Z.; Derosa, C. A.; Wang, F.; Zhuang, M.; Fraser, C. L. Phosphorescence Tuning through Heavy Atom Placement in Unsymmetrical Difluoroboron β-Diketonate Materials. *Chem. - A Eur. J.* **2018**, *24*, 1859–1869.

(74)   Daly, M. L.; Kerr, C.; DeRosa, C. A.; Fraser, C. L. Meta -Alkoxy-Substituted Difluoroboron Dibenzoylmethane Complexes as Environment-Sensitive Materials. *ACS Appl. Mater. Interfaces* **2017**, *9*, 32008–32017.

(75)   Galer, P.; Korošec, R. C.; Vidmar, M.; Šket, B. Crystal Structures and Emission Properties of the BF $_2$ Complex 1-Phenyl-3-(3,5-Dimethoxyphenyl)-Propane-1,3-Dione: Multiple Chromisms, Aggregation- or Crystallization-Induced Emission, and the Self-Assembly Effect. *J. Am. Chem. Soc.* **2014**, *136*, 7383–7394.

(76)   Lakowicz, J. R. *Principles of Fluorescence Spectroscopy*; Springer: New York, 2006.

(77)   Kochmann, S.; Baleizão, C.; Berberan-Santos, M. N.; Wolfbeis, O. S. Sensing and Imaging of Oxygen with Parts per Billion Limits of Detection and Based on the Quenching of the Delayed Fluorescence of 13C 70 Fullerene in Polymer Hosts. *Anal. Chem.* **2013**, *85*, 1300–1304.

(78)   Palmeira, T.; Fedorov, A.; Berberan-Santos, M. N. Temperature Dependence of the Phosphorescence and of the Thermally Activated Delayed Fluorescence of 12 C 70 and 13 C 70 in Amorphous Polymer Matrices. Is a Second Triplet Involved? *Methods Appl. Fluoresc.* **2014**, *2*, 035002.

(79)   Wolfbeis, O. S. Luminescent Sensing and Imaging of Oxygen: Fierce Competition to the Clark Electrode. *BioEssays* **2015**, *37*, 921–928.

(80)   Williams, D. B. G.; Lawton, M. Drying of Organic Solvents: Quantitative Evaluation of the Efficiency of Several Desiccants. *J. Org. Chem.* **2010**, *75*, 8351–8354.
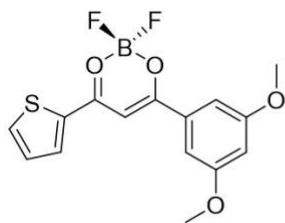
(81) Nguyen, N. D.; Zhang, G.; Lu, J.; Sherman, A. E.; Fraser, C. L. Alkyl Chain Length Effects on Solid-State Difluoroboron β-Diketonate Mechanochromic Luminescence. *J. Mater. Chem.* **2011**, *21*, 8409–8415.

(82) Demas, J. N.; Crosby, G. A. The Measurement of Photoluminescence Quantum Yields. A Review. *J. Phys. Chem.* **1971**, *75*, 991–1024.

(83) Kolpaczynska, M.; DeRosa, C. A.; Morris, W. A.; Fraser, C. L. Thienyl Difluoroboron β-Diketonates in Solution and Polylactide Media. *Aust. J. Chem.* **2016**, *69*, 537–545.

(84) Crosby, G. A.; Demas, J. N. Measurement of Photoluminescence Quantum Yields. Review. *J. Phys. Chem.* **1971**, *75*, 991–1024.

(85) Jhun, B. H.; Ohkubo, K.; Fukuzumi, S.; You, Y. Synthetic Control over Intra- and Intermolecular Charge Transfer Can Turn on the Fluorescence Emission of Non-Emissive Coumarin. *J. Mater. Chem. C* **2016**, *4*, 4556–4567.

(86) Zhang, Y.; Wang, K.; Zhuang, G.; Xie, Z.; Zhang, C.; Cao, F.; Pan, G.; Chen, H.; Zou, B.; Ma, Y. Multicolored-Fluorescence Switching of ICT-Type Organic Solids with Clear Color Difference: Mechanically Controlled Excited State. *Chem. - A Eur. J.* **2015**, *21*, 2474–2479.

(87) Shen, X. Y.; Wang, Y. J.; Zhao, E.; Yuan, W. Z.; Liu, Y.; Lu, P.; Qin, A.; Ma, Y.; Sun, J. Z.; Tang, B. Z. Effects of Substitution with Donor-Acceptor Groups on the Properties of Tetraphenylethene Trimer: Aggregation-Induced Emission, Solvatochromism, and Mechanochromism. *J. Phys. Chem. C* **2013**, *117*, 7334–7347.

(88) Haidekker, M. A.; Theodorakis, E. A. Molecular Rotors--Fluorescent Biosensors for Viscosity and Flow. *Org. Biomol. Chem.* **2007**, *5*, 1669–1678.

(89) Xiao, H.; Li, P.; Zhang, W.; Tang, B. An Ultrasensitive Near-Infrared Ratiometric Fluorescent Probe for Imaging Mitochondrial Polarity in Live Cells and in Vivo. *Chem. Sci.* **2016**, *7*, 1588–1593.

(90) Chung, K.; Kwon, M. S.; Leung, B. M.; Wong-Foy, A. G.; Kim, M. S.; Kim, J. J.; Takayama, S.; Gierschner, J.; Matzger, A. J.; Kim, J. J. Shear-Triggered Crystallization and

Light Emission of a Thermally Stable Organic Supercooled Liquid. *ACS Cent. Sci.* **2015**, *1*, 94–102.

(91)   Chen, X.; Zhang, X.; Zhang, G. Wide-Range Thermochromic Luminescence of Organoboronium Complexes. *Chem. Commun.* **2015**, *51*, 161–163.

(92)   Morris, W. A.; Kolpaczynska, M.; Fraser, C. L. Effects of α-Substitution on Mechanochromic Luminescence and Aggregation-Induced Emission of Difluoroboron β-Diketonate Dyes. *J. Phys. Chem. C* **2016**, *120*, 22539–22548.

(93)   Weissleder, R. A Clearer Vision for in Vivo Imaging. *Nat. Biotechnol.* **2001**, *19*, 316–317.

(94)   Moßhammer, M.; Strobl, M.; Kühl, M.; Klimant, I.; Borisov, S. M.; Koren, K. Design and Application of an Optical Sensor for Simultaneous Imaging of PH and Dissolved O2 with Low Cross-Talk. *ACS Sens.* **2016**, *1*, 681−687.

(95)   Koo Lee, Y. E.; Ulbrich, E. E.; Kim, G.; Hah, H.; Strollo, C.; Fan, W.; Gurjar, R.; Koo, S.; Kopelman, R. Near Infrared Luminescent Oxygen Nanosensors with Nanoparticle Matrix Tailored Sensitivity. *Anal. Chem.* **2010**, *82*, 8446–8455.

(96)   Hong, G.; Antaris, A. L.; Dai, H. Near-Infrared Fluorophores for Biomedical Imaging. *Nat. Biomed. Eng.* **2017**, *1*, 0010.

(97)   Jin, P.; Guo, Z.; Chu, J.; Tan, J.; Zhang, S.; Zhu, W. Screen-Printed Red Luminescent Copolymer Film Containing Cyclometalated Iridium(III) Complex as a High-Permeability Dissolved-Oxygen Sensor for Fermentation Bioprocess. *Ind. Eng. Chem. Res.* **2013**, *52*, 3980–3987.

(98)   Butler, T.; Wang, F.; Fraser, C. L. Controlling Solid-State Optical Properties of Stimuli Responsive Dimethylamino-Substituted Dibenzoylmethane Materials †. *Mater. Chem. Front.* **2017**, *1*, 1804–1817.

(99)   Stack, E. C.; Wang, C.; Roman, K. A.; Hoyt, C. C. Multiplexed Immunohistochemistry, Imaging, and Quantitation: A Review, with an Assessment of Tyramide Signal Amplification, Multispectral Imaging and Multiplex Analysis. *Methods* **2014**, *70*, 46–58.

(100) Yu, X.; Ge, X.; Lan, H.; Li, Y.; Geng, L.; Zhen, X.; Yi, T. Tunable and Switchable Control of Luminescence through Multiple Physical Stimulations in Aggregation-Based Monocomponent Systems. *ACS Appl. Mater. Interfaces* **2015**, *7*, 24312–24321.

(101) Jangwon, S.; Kim, S.; Park, S. Y. Strong Solvatochromic Fluorescence from the Intramolecular Charge-Transfer State Created by Excited-State Intramolecular Proton Transfer. *J. Am. Chem. Soc.* **2004**, *126*, 11154–11155.

(102) Klymchenko, A. S. Solvatochromic and Fluorogenic Dyes as Environment-Sensitive Probes: Design and Biological Applications. *Acc. Chem. Res.* **2017**, *50*, 366–375.

(103) Zhang, G.; Lu, J.; Fraser, C. L. Mechanochromic Luminescence Quenching: Force-Enhanced Singlet-to-Triplet Intersystem Crossing for Iodide-Substituted Difluoroboron−Dibenzoylmethane−Dodecane in the Solid State. *Inorg. Chem.* **2010**, *49* , 10747–10749.

(104) Sun, X.; Wang, X.; Li, X.; Ge, J.; Zhang, Q.; Jiang, J.; Zhang, G. Polymerization-Enhanced Intersystem Crossing: New Strategy to Achieve Long-Lived Excitons. *Macromol. Rapid Commun.* **2015**, *36*, 298–303.

(105) Zhou, C.; Xie, T.; Zhou, R.; Trindle, C. O.; Tikman, Y.; Zhang, X.; Zhang, G. Waterborne Polyurethanes with Tunable Fluorescence and Room-Temperature Phosphorescence. *ACS Appl. Mater. Interfaces* **2015**, *7*, 17209–17216.

TOC Graphic:

Difluoroboron β-Diketonate

Heavy-Atom Free Phosphorescence

*PLA film

N_2